CHEMISTRY OF MATERIALS

pubs.acs.org/cm

Article

Hackmanite—The Natural Glow-in-the-Dark Material

Cecilia Agamah,▲ Sami Vuori,▲ Pauline Colinet, Isabella Norrbo, José Miranda de Carvalho, Liana Key Okada Nakamura, Joachim Lindblom, Ludo van Goethem, Axel Emmermann, Timo Saarinen, Tero Laihinen, Eero Laakkonen, Johan Lindén, Jari Konu, Henk Vrielinck, David Van der Heggen, Philippe F. Smet, Tangui Le Bahers,* and Mika Lastusaari*

Cite This: https://dx.doi.org/10.1021/acs.chemmater.0c02554

Read Online

ACCESS | Metrics & More | Article Recommendations | Supporting Information

ABSTRACT: "Glow-in-the-dark" materials are known to practically everyone who has ever traveled by airplane or cruise ship, since they are commonly used for self-lit emergency exit signs. The green afterglow, persistent luminescence (PeL), is obtained from divalent europium doped to a synthetic strontium aluminate, but there are also some natural minerals capable of afterglow. One such mineral is hackmanite, the afterglow of which has never been thoroughly investigated, even if its synthetic versions can compete with some of the best commercially available synthetic PeL materials. Here we combine experimental and computational data to show that the white PeL of natural hackmanite is generated and controlled by a very delicate interplay between the natural impurities present. The results obtained shed light on the PeL phenomenon itself thus giving insight into improving the performance of synthetic materials.

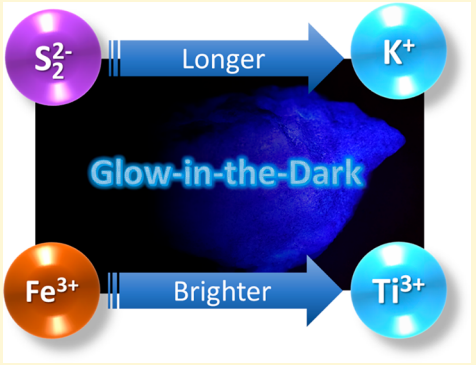

INTRODUCTION

Hackmanite is a mineral with the general composition $Na_8Al_6Si_6O_{24}(Cl,S)_2$. It is typically formed in low-silica and alkaline magmas.[1] Such conditions are present in nepheline syenites, phonolites, and related rock types, in metasomatized calcareous rocks as well as in cavities of ejected volcanic blocks.[2] Hackmanite is known for its ability to show purple tenebrescence, i.e., reversible photochromism, upon UV and X-ray exposure.[3] Because of this property, natural hackmanite has found use as, e.g., a gemstone,[4] whereas artificial hackmanites are considered for high-tech applications such as UV dose monitoring.[5] Hackmanite is no longer accepted as an official mineral name by the International Mineralogical Association,[6] so in view of its property, photochromic or tenebrescent sodalite could be a more proper name. However, for consistency with previous publications, we will keep using the name hackmanite in this work. The mechanism of tenebrescence in hackmanites is now established to be due to a UV stimulated electron transfer from S_2^{2-} ions to chloride vacancies creating color centers that absorb in the visible range.[7] The electrons can transfer back to the disulfide if enough thermal or optical energy is given.[5,8,9]

Hackmanite also shows characteristic orange/red luminescence under UV irradiation due to the $^2\Pi_u \rightarrow {}^2\Pi_g$ transition of S_2^- entities.[10] This is observed as a wide band spanning from ca. 500 to 800 nm and showing a vibronic structure with a ca. 560 cm^{-1} peak separation[11,12] also observed in other aluminosilicate minerals like haüyne ($Na_3CaSi_3Al_3O_{12}SO_4$),[13−16] nosean ($Na_8Al_6Si_6O_{24}SO_4$),[13−16] and scapolite ($(Na,Ca)_4(Al,Si)_3Si_6O_{24})(Cl,CO_3)$).[17,18] In natural hackmanites, impurity ions such as Fe^{3+} or Cr^{3+} (red emission) and s^2 type centers (blue emission) have also been reported to give luminescence.[10] The blue band has been reported to show "an afterglow of several seconds"[10] or "prolonged afterglow of white light".[19] Such an afterglow is often called phosphorescence by mineralogists, but here we use the term persistent luminescence (PeL) because the afterglow is not due to forbidden transitions (as is the case with phosphorescence) but it is caused by the trapping of charge carriers and their slow release. Therefore, persistent luminescence will always last longer than the emission lifetime of the emitting ion, i.e., PeL can persist up to hours. In hackmanites, PeL is not present in every natural sample. Other minerals showing persistent luminescence include, e.g., fluorite (CaF_2), sphalerite (ZnS), calcite and aragonite ($CaCO_3$), gypsum ($CaSO_4{\cdot}2H_2O$), willemite (Zn_2SiO_4), Barite ($BaSO_4$), creedite ($Ca_3Al_2(SO_4)(F,OH)_{10}{\cdot}2(H_2O)$), and wollastonite ($CaSiO_3$).[20,21]

Recently, some of us reported the exceptionally long PeL in synthetic Ti^{3+} doped $(Li,Na)_8Al_6Si_6O_{24}(Cl,S)_2$ hackmanite.[22] The emission stays up to 7 h above the luminance limit of 0.3

Received: June 18, 2020
Revised: September 25, 2020
Published: September 25, 2020

Table 1. Overall Elemental Compositions (In Weight%) of the Studied Samples Based on XRF Analyses[a]

element	nominal	synthetic	Greenland	Koksha V.1	Koksha V.2	Mt. St. Hilaire	Pakistan
Na	32.03	26.4(1)	20.0(3)	21.0(1)	18.5(1)	17.7(30)	24.2(5)
Al	28.19	27.4(1)	29.5(1)	29.3(1)	30.6(9)	28.1(13)	29.3(2)
Si	29.35	30.2(1)	31.6(1)	30.5(1)	33.3(1)	33.0(1)	28.4(1)
Cl	9.88	11.9(1)	17.7(1)	17.5(1)	16.9(1)	19.1(1)	14.7(1)
S	0.56	0.46(2)	0.80(0)	0.30(0)	0.30(0)	0.13(0)	0.24(0)
Mg							0.90(0)
K		1.5(1)		0.84(0)	0.0(0)	0.16(0)	0.83(0)
Ca			0.06(0)	0.31(0)	0.15(0)	0.04(0)	0.69(0)
Ti		2.1(1)	0.05(0)	0.04(0)	0.0(0)	0.0(0)	0.06(0)
V					0.16(0)		
Cr							
Mn					0.02(0)	0.13(0)	
Fe			0.11(5)	0.05(0)	0.03(0)	1.13(0)	0.08(0)
Ni					0.02(0)	0.01(0)	
Cu						0.01(0)	
Zn			0.09(0)			0.03(0)	0.03(0)
Ga			0.08(0)	0.03(0)	0.02(0)	0.02(0)	0.05(0)
Ge					0.03(0)	0.01(0)	
Br			0.05(0)	0.04(0)	0.1(0)	0.16(0)	0.20(0)
Sr					0.0(0)		
Zr						0.02(0)	
Pd							0.24(0)
Cs						0.10(0)	
La			0.08(0)	0.05(0)			0.11(0)
Nd						0.14(0)	
Tl						0.02(0)	

[a]The nominal composition for a typical hackmanite $Na_8Al_6Si_6O_{24}Cl_{1.6}S_{0.1}$ is given as well. Esds are given in parentheses.

mcd/m^2 which is set as the standard limit by DIN 67510−1:2009−11[23] in the self-lit exit sign industry. All the synthetic hackmanites exhibiting PeL (see refs 9, 22, and 24) show a similar blue/white emission as that reported for natural hackmanite,[10] and this has been attributed to be due to ppm level titanium impurities and oxide vacancies (V_O). Together, these create emitting Ti^{3+}−V_O pairs with the mechanism being such that (1) the Ti^{3+} absorbs excitation energy which allows the transfer of an electron to the V_O acting as a trap, (2) thermal energy available at room temperature lifts the electron away from the trap back to the Ti^{3+} again, and (3) emission is as a charge transfer toward the Ti^{3+}.[22]

Motivated by the possibility of boosting the design of new materials by studying the rich and diverse framework of natural hackmanites, we set out to investigate why only some natural hackmanites show persistent luminescence. Consequently, we present for the first time a quantitative characterization of the PeL and optical energy storage properties in natural hackmanites. We study five natural hackmanite samples, from (1) Greenland, (2) Mont Saint Hilaire (Canada), (3) Koksha Valley sample 1 (Afghanistan), and (4) Koksha Valley sample 2 (Afghanistan) as well as (5) Pakistan, and compare their properties with those of a synthetic Ti^{3+} doped $(Li,Na)_8Al_6Si_6O_{24}(Cl,S)_2$ hackmanite. On the basis of experimental and quantum chemical characterization of these minerals, we will demonstrate interplays between the nature and concentration of several impurities and the PeL phenomenon.

MATERIALS AND METHODS

The natural hackmanites were obtained from private collectors. The synthetic $(Li,Na)_8Al_6Si_6O_{24}(Cl,S)_2$:$Ti^{3+}$ hackmanite was synthesized as reported in ref 22: Dried Zeolite A (0.7000 g, Sigma-Aldrich, product no. 96096), Na_2SO_4 (0.0600 g, E. Merck, 99%), NaCl (0.1175 g, J. T. Barker, 99.5%) and LiCl (0.0850 g, Acros, 99%) powders were mixed together with TiO_2 (0.0060 g, Merck, 99%) powder. Ten weight-% of H_3BO_3 (Merck, > 99.8%) was added as a flux. The mixture was first heated at 850 °C for 48 h. The product was allowed to freely cool down to room temperature and ground. Finally, the product was reheated at 850 °C for 2 h under a flowing 12% H_2 + 88% N_2 atmosphere.

Crystal structure and purity were checked with X-ray powder diffraction measurements using a Huber G670 position sensitive detector and $CuK_{\alpha 1}$ radiation (λ = 1.540 60 nm). Elemental composition was investigated using a Bruker Tornado M4 micro-XRF spectrometer (Table 1, Figure S5 of the Supporting Information, SI) or a PANalytical Epsilon 1 (Table S2) device.

Photoluminescence was visually checked using hand-held UV lamps UVP UVLS-24 operating with 4 W at 254 or 365 nm as well as UVP UVM-57 operating with 6 W at 302 nm. These lamps give an irradiance of 5.8, 6.4, and 4.3 mW/cm^2, respectively, on the surfaces of their exit windows. Photoluminescence emission spectra were measured at room temperature with LED excitation using Roithner models UVTOP255 (255 nm), UVTOP295 (295 nm) and UVTOP355 (355 nm). The LEDs were operated at 20 mA, which corresponds to an approximate power of 0.5 mW. An Avantes Avaspec HS-TEC spectrometer connected to a 600 μm optical fiber was used to collect the spectra. Cathodoluminescence was studied at room temperature with a Nuclide Corporation ELM2EX Luminoscope equipped with a Nuclide Corporation ELM2B vacuum chamber coupled to the same spectrometer with the same fiber. The spectra were corrected for the sensitivity of the setup. The rise of the blue photoluminescence emission was recorded with the same spectrometer and fiber using the 295 nm LED described above at 0.35 mW/cm^2 irradiance. The irradiance was determined with an Opsytec Dr. Gröbel Radiometer RM 12 equipped with a RM12 sensor calibrated for UVB. The irradiance level was controlled by adjusting the distance between the lamp and the hackmanite material. Photoluminescence

https://dx.doi.org/10.1021/acs.chemmater.0c02554
Chem. Mater. XXXX, XXX, XXX−XXX

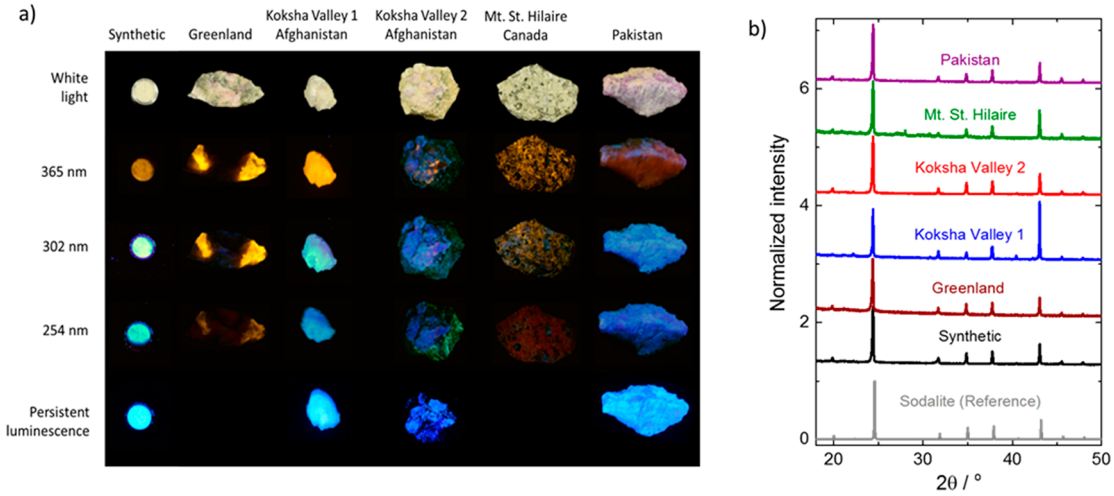

Figure 1. (a) Photos of the samples used in this study: under white light, 365, 302, and 254 nm and their persistent luminescence. Note that the sample sizes seen in the photo are not comparable, because the zoom settings were different for each sample so that each sample would fill the picture frame. (b) X-ray powder diffraction patterns of the samples taken from orange-emitting parts. The reference pattern for sodalite[37] is given in the bottom.

excitation spectra were measured using the Varian Cary Eclipse spectrometer described above. Photos of the two additional Koksha Valley samples discussed in connection with persistent luminescence were taken under irradiation by a UVTao Yuan 20 LED array equipped with a U325 filter (275 nm, 80 mW) and Convoy S2+ LED torch equipped with a ZWB2 filter (365 nm, 300 mW).

Persistent luminescence fading was quantified with a Hagner ERP-105 luminance photometer (with Hagner SD 27 detector) after exciting the samples for 30 min at 302 nm (UVP UVM-57, 6 W) equaling to a dose of 36 kJ/m^2. Persistent luminescence spectra were measured with an Avantes AvaSpec HS-TEC spectrometer 1 min after ceasing a 2 min irradiation with the 302 nm hand-held UV lamp described above. The spectra were corrected for the sensitivity of the setup. Reflectance spectra were measured with a Konica Minolta CM-2300d spectrophotometer using D65 illuminant and 10° observer. For the persistent luminescence excitation spectrum, the sample was irradiated with a Varian Cary Eclipse Fluorescence Spectrophotometer equipped with a Hamamatsu R928 PMT (photomultiplier) and a 150 W xenon lamp for 1 min with the chosen wavelength. Then, the emission spectrum was measured (data collection time: 4 s for the whole spectrum) 1 min after the irradiation was stopped. After this, a fresh sample was introduced, the irradiation wavelength was changed and the procedure was repeated. The intensity values were obtained by integrating over 400−700 nm at each irradiation wavelength. Thermoluminescence (TL) glow curves were measured with a MikroLab Thermoluminescent Materials Laboratory Reader RA'04 using a heating rate of 10 °C/s. Aluminum sample cups were used. Prior to the measurements, the samples were irradiated at room temperature for 1 min with 254 nm (UVP UVGL-25, 4 W) and the TL measurements were started 20 s after ceasing the irradiation. The glow curves were analyzed using the initial rise method[25] after correcting the glow curves for thermal quenching. Thermogravimetric measurements were carried out with a TA Instruments Q600 device in flowing air (100 cm^3/min) with a heating rate of 10 °C/min. Alumina sample cups were used.

Photon counting experiments to determine the storage capacity were carried out using the procedure outlined in.[26]A hand-held UV lamp operating with 8 W at 302 nm was used to excite the hackmanite during 25 min before the PeL was recorded.

Elemental distributions in the hackmanite grains were studied with SEM-EDX point analyses (50 points per sample) using a Leo 1530 Gemini microscope equipped with a Thermo Scientific UltraDry SDD EDS system. Statistical analysis on the compositions in those points was carried out using the IBM SPSS Statistics 24.0 software.

Computational Details and Methodology. The simulation of energy levels of all the defects considered is performed by combining DFT periodic boundary condition calculations to obtain geometries around the defects and TD-DFT calculations performed on cluster centered on the defect using a molecular approach. Briefly, all geometry optimizations in the periodic boundary condition were performed with the CRYSTAL17 code[27] along with the global hybrid functional PBE0[28] which is known to give accurate geometrical parameters for sodalites.[7] A 12 × 12 × 12 k-points mesh was used for the geometry optimization of the bulk system while the Γ point was used for geometry optimization of the 2 × 2 × 2 supercell containing the defect. All-electron double-ζ basis sets with polarization functions were used for Si, Al, O, K, Na, and Cl atoms. For titanium and iron, pseudopotentials are used to exclude the atomic core electrons. The S atoms were treated by an all electron triple-ζ basis set while an optimized triple-ζ basis set was used for the electron trapped in a vacancy. The convergence criterion for the SCF cycle was fixed at 10^{-8} Ha per unit cell. All TD-DFT calculations performed on a cluster extracted from the PBC calculations are performed using the Gaussian16[29] code with the cam-B3LYP functional[30] and using the 6-31G(d) basis set. The cluster is embedded in a point charge cloud simulating the Madelung potential of the crystal. More computational details and information on the computational methodology, especially on the choice of the cluster size and embedding, are given in the SI.

Mössbauer spectra were recorded with a Doppler velocity of ∼2.0 mm/s and calibrated with α-Fe. Spectra were measured in transmission geometry at 77.6 and 300 K using an Oxford CF506 continuous-flow cryostat with liquid N_2 as coolant and a ^{57}Co:*Rh* source (Ritverc Co. Twenty-five mCi June 2018). The spectra were fitted using a nonlinear least-squares fitting program with the following Mössbauer parameters released in the fitting: the quadrupole coupling constant eQV_{zz}, the relative component intensities, and the isomer shift δ relative to α-Fe.

X-band (9.54 GHz) EPR spectra were recorded at room temperature on a Varian E-line spectrometer with a standard rectangular cavity. The microwave frequency was measured with a HP 5342A frequency counter. Magnetic fields were measured with a Bruker B-NM12 NMR oscillator and calibrated against the EPR signal of diphenyl picryl hydrazyl (DPPH, g = 2.0036). Q-band (34.00 GHz) EPR spectra were recorded with a Bruker Elexsys E500 spectrometer with a cylindrical QTE cavity. The microwave frequency was measured with a Pendulum CNT-90XL frequency counter and fields with a Bruker ER035 M Gaussmeter. The magnetic fields were calibrated against the $g_\perp$ component of the CO_3^{3-} radical in irradiated calcite powder (g = 2.0031).[31] Room temperature spectra were

https://dx.doi.org/10.1021/acs.chemmater.0c02554
Chem. Mater. XXXX, XXX, XXX−XXX

recorded under normal air atmosphere. It was checked (X-band) that reducing the pressure by evacuating the sample tube (<10 mbar) has no significant influence on the spectrum. For measurements at low temperatures the Q-band spectrometer is equipped with a QTE CF910 He-flow cryostat (2−300 K, Oxford Instruments).

RESULTS AND DISCUSSION

Initial Characterization. As the first step, the five natural samples claimed to be hackmanite were placed under UV lamps to see if they show the emission colors typical of hackmanite and if persistent luminescence was present. Indeed, under 365 nm excitation some parts of all samples showed an orange/red emission that could be due to the disulfide group (Figure 1a). Some of them also showed the blue/white emission under excitation at 302 and/or 254 nm and three of them showed persistent luminescence. Since hackmanites are defined as being photochromic sodalites and since the photochromism is due to the disulfide group which also shows orange photoluminescence, we chose such parts of the samples that showed the disulfide emission for further characterization (please see the SI file for a detailed description of the homogeneity of the samples). These parts were removed and powdered from the rocks with a diamond-covered carbide drill bit for further analysis. Routine X-ray powder diffraction measurements indicated that all these samples possessed the sodalite structure (Figure 1b), which is cubic with space group $P\bar{4}3n$ (No. 218) and unit cell axis length of ca. 8.9 Å.[8] The structure consists of a framework of four- and six-membered rings of alternating AlO_4 and SiO_4 tetrahedra. $(Na_4Cl)^{3+}$ entities are situated within the cavities of the structure, and Na is coordinated to three O^{2-} ions from the framework and one Cl^-. S_2^{2-} ions substitute some of the Cl^- ions, which results in chloride vacancies to balance the charge.[8] The elemental composition determined with XRF is presented in Table 1.

Photoluminescence and Cathodoluminescence. First, we studied all samples for regular photoluminescence. We chose to use wavelengths 255 and 355 nm as excitation wavelengths because those are close to the 254 and 365 nm that are readily available from hand-held UV lamps. Furthermore, we used 295 nm excitation, because that has been observed to efficiently excite the persistent luminesence of synthetic hackmanites.[22] With excitation at 355 nm, all samples only show the characteristic orange emission of S_2^- entities[10] (Figure 2a). The bands are centered at around 615 nm and they present the expected vibronic contributions with ca. 550 cm^{-1} separation as recently confirmed by quantum chemical calculations.[12] The spectra of the Koksha Valley 2 and Pakistan samples seem to be red-shifted, but what appears to be a shift is actually an effect of self-absorption. These two samples have a distinct purple body color and thus they absorb strongly around 550 nm (see Figure 1a and reflectance spectra presented later), causing a deletion of the high-energy side of the emission spectrum. With excitation at 295 nm, the blue/green emission peaking at ca. 500 nm appears in most samples, but in the Mt. St. Hilaire sample this blue band is weak and in the Greenland sample only the S_2^- emission is observed (Figure 2b). According to previous reports, we assign the blue/green emission to the Ti^{3+}−V_O pair.[9,22] Furthermore, each sample also shows the orange peak overlapping with the blue/green one and the Mt. St. Hilaire sample presents a red band at 720 nm. According to Gaft et al.[10] this red band can be assigned to either Fe^{3+} or Cr^{3+} residing at the Al^{3+} site. Our

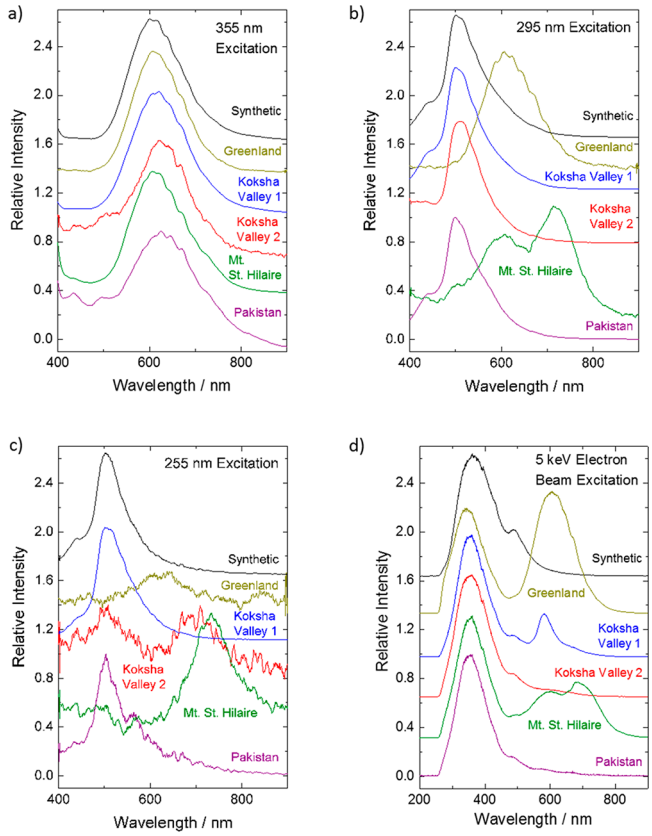

Figure 2. Photoluminescence spectra upon continuous LED excitation at (a) 355, (b) 295, and (c) 255 nm as well as (d) cathodoluminescence spectra. All spectra are measured from ground parts of the samples where the disulfide emission was present.

XRF data (Table 1) suggest that the concentration of Cr is zero or at least below the detection limit of the method, whereas Fe is clearly present in all the natural samples. Thus, we assign this red emission band to Fe^{3+}. Then, we used 255 nm to excite the samples (Figure 2c) and observed the blue/green emission band for all other samples except the Greenland and Mt. St. Hilaire ones. The Greenland sample still only shows the disulfide emission, whereas the Mt. St. Hilaire sample shows only the 720 nm peak. Finally, cathodoluminescence spectra (Figure 2d) show a combination of all the signals discussed above as well as a strong UV/blue band peaking at 350 nm for the natural samples and at 364 nm for the synthetic one. To test where this peak originates from, we also measured the cathodoluminescence spectra of nondoped Al_2O_3, SiO_2, and Zeolite A (approximate composition: $NaAlSiO_4$), which showed this peak both for Zeolite A and Al_2O_3 (Figure S1). Thus, in line with previous reports on the luminescence of α-Al_2O_3, we assign this band to an F^+ center,[32−34] i.e., an oxygen vacancy occupied with one electron, in the vicinity of Al^{3+}. In this same band, one can also observe small glitches at 359, 393, and 432 nm, which can be assigned to the transitions of small amounts of N_2 and Ar present in the measurement chamber.[35] As a further test of the origin of the UV band, we measured the cathodoluminescence spectrum of the synthetic and the Pakistan samples as a function of time. While the rest of the emission band intensities seem to remain constant, that of the UV band decreases with increasing time in the electron beam (Figure S2) indicating that the concentration of F^+ centers decreases.

https://dx.doi.org/10.1021/acs.chemmater.0c02554
Chem. Mater. XXXX, XXX, XXX−XXX

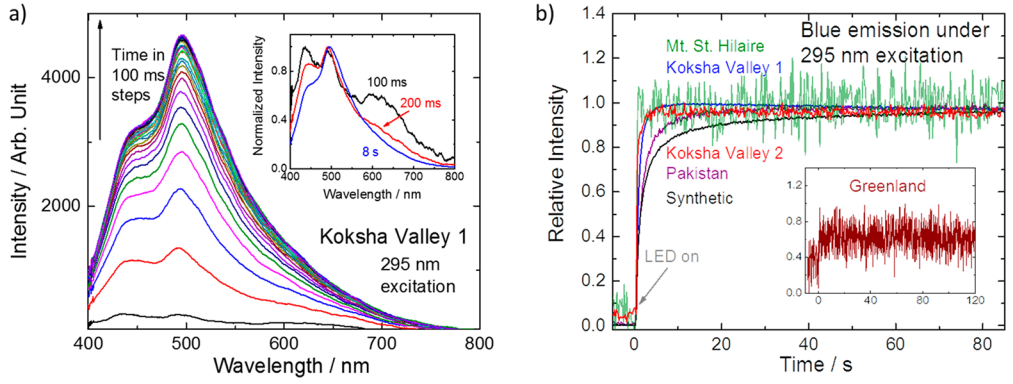

Figure 3. (a) Photoluminescence spectra of the Koksha Valley sample 1 measured with 100 ms steps after starting excitation. (b) Rise curves of the blue emission for all samples. Due to its weak emission intensity and thus high noise level, the rise curve of the Greenland sample is shown in the inset only.

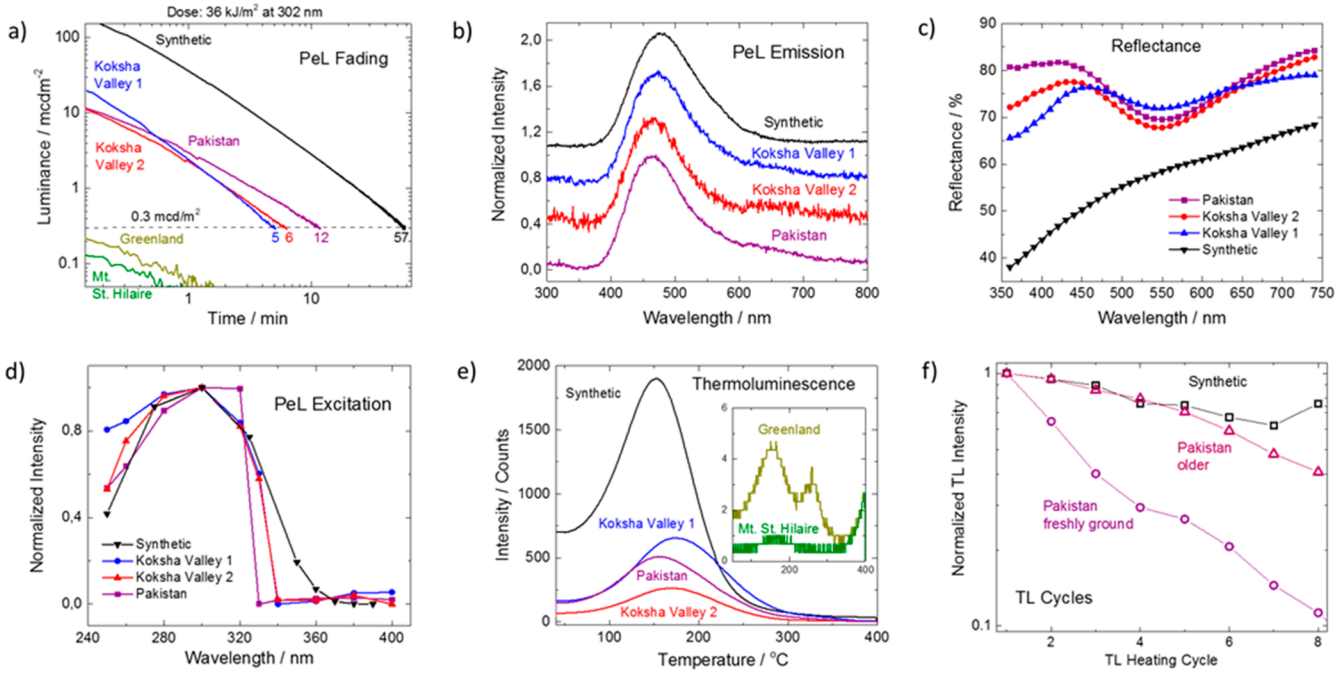

Figure 4. (a) PeL fading curves, (b) PeL emission spectra, (c) reflectance spectra before any UV exposure or heating, (d) PeL excitation spectra, and (e) thermoluminescence glow curves (measured with a delay of 20 s between the ceasing of irradiation and measurement) of the natural and synthetic samples. (e) Glow curves of the Greenland and Mt. St. Hilaire samples are shown in the inset because of their low intensity. (f) Effect of repeated charging/heating cycles on the TL signal of the synthetic and Pakistan samples.

Previously, it has been reported that prolonged electron irradiation converts F centers (two electrons in an oxygen vacancy) to F^+ centers,[36] i.e., the irradiation removes electrons from oxygen vacancies. Since we observed a decrease in the F^+ center emission, we suggest that this indicates that the F^+ centers are being converted to nonluminescent F^{2+} centers, i.e., the concentration of completely empty oxygen vacancies increases.

It is interesting to note that the synthetic, Pakistan as well as Koksha Valley samples 1 and 2 appear first orange under 295 nm excitation and then change to blue/white. This is due to the slow rise time of the blue/green emission in these samples. As an example, we present the time-dependent photoluminescence spectra of the Koksha Valley sample 1, which show that within the first few 100 ms the blue emission becomes intense enough to beat the orange one (Figure 3a). The rise of the blue emission is slow, because in the beginning the absorbed photons are used to store electrons to electron traps. Once the traps are filled, the emission intensity reaches saturation. Because of such traps, these four samples show blue/white persistent luminescence. If we compare the time that it takes to reach saturation in emission intensity with PeL decay time (to be discussed later), then we can observe an almost linear dependence between them (Figure S3). For the other samples, the blue/green emission rises much faster (Figure 3b) and no PeL is observed from them.

Persistent Luminescence and Energy Storage Properties. The preliminary UV lamp tests (Figure 1) indicated that only the Koksha Valley 1 and 2 as well as Pakistan samples showed persistent luminescence. Nevertheless, we measured the luminance fading curves for all samples after 30 min of irradiation at 302 nm. The results (Figure 4a) indicate that the Pakistan sample shows PeL above the 0.30 mcd/m^2 limit up to 12 min, the Koksha Valley 2 sample up to 6 min and the

https://dx.doi.org/10.1021/acs.chemmater.0c02554
Chem. Mater. XXXX, XXX, XXX−XXX

Koksha Valley 1 sample up to 5 min, whereas the synthetic sample used as reference glows 57 min above this threshold value. The luminance radiometer was also able to detect that both the Greenland and Mt. St. Hilaire samples do show PeL, but the intensity is below the 0.30 mcd/m^2 limit already in the beginning of the measurements.

The persistent emission peaks in the range of 465−475 nm for the natural samples (Pakistan, Koksha Valley 1 and 2) as well as the synthetic one (Figure 4b). The PeL bands of the natural samples seem to be narrower from the high wavelength side than that of the synthetic material. This is due to the purple body color of the natural samples as opposed to the yellowish appearance of the synthetic sample, i.e., the natural samples have an absorption band at around 550 nm (shown as a minimum in the reflection spectra; Figure 4c), whereas the synthetic sample has no clear absorption maxima. In addition to the PeL emission spectra of the natural and the synthetic samples being very similar also their PeL excitation spectra are quite similar, peaking at ca. 300 nm (Figure 4d). The one difference is that the natural samples' excitation peaks are narrower and steeper on the high wavelength side. This is due to the absorption by Fe^{3+} in the natural samples as we show later. Nevertheless, the similarity in the PeL emission and excitation suggests that the PeL emitter is the same in all samples, i.e., the Ti^{3+}−V_O pair as reported previously for synthetic hackmanite.[22]

Thermoluminescence glow curves (Figure 4e) show rather intense single peaks with maxima between 150 and 180 °C for the synthetic, Pakistan, Koksha Valley 1 and 2 samples. For the Greenland and Mt. St. Hilaire samples, the same peak is observed, but with much lower intensity. In addition, a peak at 250 °C is present for the Greenland sample. The TL intensities correlate rather well with the PeL intensity fading curves (Figure 4a) considering that the TL measurements were started with a 20 s delay from the irradiation. Initial rise fits indicate that the depth of the trap corresponding to the main TL peak ranges from 0.39 (synthetic) to 0.47 eV (Koksha Valley 1) suggesting that also the trap structure is rather similar between the studied samples. It must be noted that the TL signal of the Mt. St. Hilaire sample was too low for a reliable initial rise fit, but the resulting value 0.33 eV is still close to those of the other samples.

We noticed that the TL intensity almost dies with repeated charging-heating cycles for natural hackmanite, while the synthetic one withstands such cycles much better. Here, we use the Pakistan sample as an example and its TL falls 95% during 10 consecutive charging/heating cycles up to a temperature of 400 °C, whereas the synthetic one suffers a quench of approximately 40% (Figure 4f). However, when a similar experiment is done for the natural sample months after drilling the powder sample off the original rock, the behavior is very similar to that of the synthetic one (Figure 4f). Although the difference between the freshly powdered and older Pakistan sample is very high, the difference between the initial TL intensity in these two tests is negligible (Figure S4a). Additional thermogravimetric analyses (Figure S4b) suggested that there is a small loss of weight for both the Pakistan sample (ca. 2%) and the synthetic one (ca. 1%) between room temperature and 400 °C (upper limit of our TL measurements). However, X-ray powder diffraction (Figure S4c) and XRF measurements (Table S1) indicated that neither the crystal structure nor the overall elemental composition changes due to heating. These results thus suggest that the decrease of TL performance in repeated measurements is due to changes in the defect structure rather than the bulk structure. The changes could be, e.g., the oxidation of Ti^{3+} (the PeL emitter) to Ti^{4+}, filling of oxygen vacancies (where energy is trapped in the TL mechanism) or oxidation of Fe^{2+} to Fe^{3+} (PeL quenching; see the section on the interplay between titanium and iron). It seems that the freshly powdered sample's defects are overall in a metastable state that is affected far more by heating than a sample that has reached an equilibrium with ambient conditions.

To compare the energy storage capabilities of the synthetic and natural materials, we carried out photon counting measurements for the synthetic and Pakistan (old) samples following the procedure described earlier by some of us.[26] The results were consistent with the PeL fading curves (Figure 4a) indicating a capacity of 2.8×10^{15} photons/g for the synthetic sample and 3.1×10^{14} photons/g for the Pakistan one. These values are very much in the same magnitude that has been reported for CaS:Eu nanoparticles (7.3×10^{14} photons/g)[26] but much lower than that reported for the most efficient synthetic PeL material $SrAl_2O_4$:Eu,Dy (1.6×10^{17}).[26] Previously, we reported that the concentration of color centers in a synthetic tenebrescent hackmanite was experimentally determined to be ca. 10^{16} per gram,[5] whereas for natural hackmanites the value can be, e.g., 6×10^{17} per gram. The latter value was calculated with the equation given by van den Brom et al. (eq 12 in ref 38) and the oscillator strength of 0.3 au reported for the absorption of the color center.[7] Therefore, it seems that natural hackmanites are much more efficient in tenebrescence than persistent luminescence.

Why Do Not All Natural Hackmanites Show Noticeable Persistent Luminescence? As discussed above, it seems that if natural hackmanite shows any blue emission, it will also show persistent luminescence. We know that this emission is originating from titanium, but judging from the Ti contents presented in Table 1, there seems to be no connection between Ti concentration and PeL. A similar conclusion can be drawn from the XRF elemental mapping that we carried out for another hackmanite sample from Greenland that has regions with and without the blue emission, i.e., the blue-emitting regions do not have any different Ti contents than the other parts of the sample (Figure S5). However, all the XRF results give only a micrometer scale resolution. Thus, to reach the nanometer scale, we carried out SEM-EDX measurements for 50 random points in each natural sample. The obtained elemental contents were normalized and a principal component analysis followed by ANOVA (analysis of variance) were carried out on the contents. The details of the analyses are discussed in the SI file.

The statistical analyses suggested that there are two important pairs of elements whose concentrations correlate with persistent luminescence: K and S as well as Ti and Fe. More specifically, higher values of c(K)−c(S) (i.e., difference between the concentrations of K and S) and c(Ti)−c(Fe) indicate that there is persistent luminescence and low values indicate the lack of persistent luminescence. That is, the more there is K in comparison with S the more likely it is to get PeL. Similarly, the more there is Ti in comparison with Fe the more likely it is to get PeL. These possible correlations are well witnessed in such natural hackmanite samples that show an uneven distribution of emission intensity/color or tenebrescence: places showing a more intense orange luminescence usually show no PeL or stronger tenebrescence and often these

https://dx.doi.org/10.1021/acs.chemmater.0c02554
Chem. Mater. XXXX, XXX, XXX−XXX

places have a brown tinge from Fe^{2+} or show a red Fe^{3+} luminescence (Figure 5). Below, we will discuss the effects of these element pairs in more detail.

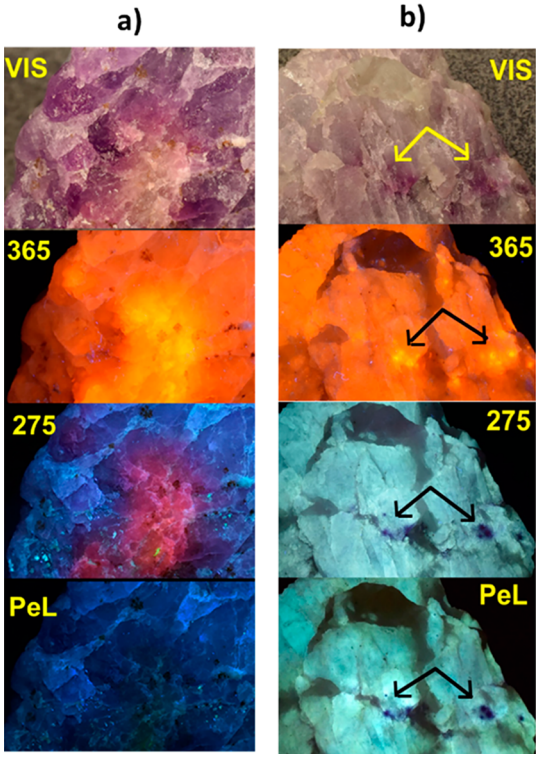

Figure 5. Photos of two additional hackmanite samples from Koksha Valley with uneven distribution of emitters and emission intensity as well as tenebrescence. (a) Areas with intense orange disulfide emission (365 nm excitation) and Fe^{3+} emission (275 nm excitation) show negligible PeL. (b) Spots indicated by arrows show strong tenebrescence and strong disulfide emission (365 nm excitation) but weak blue/green emission (275 nm excitation) and weak PeL.

Interplay between Titanium and Iron. It is assumed that Ti^{3+} is involved both in the absorption and emission parts of PeL.[9,22] This assumption is based on the fact that increasing the titanium concentration in synthetic hackmanite will increase the intensity of both the blue PL and PeL. To the best of the authors' knowledge, there is no other literature on Ti^{3+} in tetrahedral sites in oxides and thus literature cannot be used to back up that assumption. Therefore, we carried out energy levels quantum chemical calculations for Ti^{3+} ($Ti_{Al}^{\times}$) and Ti^{4+} ($Ti_{Si}^{\times}$) in hackmanite. The calculated data (Figure 6a) indicates that an electron can be excited from Ti^{3+} to the conduction band with ca. 3.7 eV (335 nm), which agrees very well with the PeL excitation threshold energy (ca. 3.9 eV/320 nm; Figure 4d). Moreover, this complies with the common understanding that PeL is initiated with electron transfer from the absorbing ion to the conduction band. The results also suggest that Ti^{4+} is not the absorbing ion since its only transition ($O^{2-} \rightarrow Ti^{4+}$) requires more than 5 eV (less than 248 nm). The computational data thus confirm that it is indeed Ti^{3+} that is excited through a charge transfer transition in the PeL mechanism. Furthermore, the blue emission corresponds to the back charge transfer from the conduction band to Ti^{3+}, and not d-transition of Ti^{3+} that is computed in the near IR around 1.2 eV. With the role of Ti^{3+} established and because Fe^{2+} is a well-known ominous luminescence quencher,[39] the importance of the interplay between titanium and iron seems rather obvious. Thus, it is to be expected that increased Fe concentration will require increased Ti concentration to enable PeL. Below, we will discuss in more detail how iron affects the blue luminescence and PeL in hackmanites.

First, to find out which oxidation states of iron are prominent, we carried out a Mössbauer measurement (Figure 6b) for the Mt. St. Hilaire sample, which shows the highest Fe content (Table 1) and shortest PeL (Figure 4a). Due to the low concentration of iron (ca. 1 wt %), the signals were rather weak and thus even the component due to Fe traces in the gamma detector was visible (gray dashed line). The spectrum is dominated by a quadrupole doublet assigned to high-spin Fe^{3+} (red). Another weaker doublet is also compatible with high-spin Fe^{3+} (green). Probably, the two components occupy separate cation sites, i.e., Al^{3+} and Si^{4+} sites. The results thus indicate that Fe^{3+} is the dominant species, but the presence of some Fe^{2+} cannot be ruled out completely. This is because concentrations that are below the detection limit of Mössbauer may still be optically functional. The experimentally obtained hyperfine parameters are given in the SI (Table S7). EPR measurements on the Mt. St. Hilaire sample confirm the presence of Fe^{3+}, with spectral characteristics similar to those observed for Fe^{3+} in sodalite[40] (see SI for details). Fe^{2+}, that has only rarely been detected with EPR, was not observed in these experiments.

Since the Mt. St. Hilaire sample shows the emission band of Fe^{3+} at 720 nm (Figure 2), we could record the photoluminescence excitation spectrum of Fe^{3+} in hackmanite (Figure 6c). In the spectrum, one can observe weak d-d transitions at the same wavelengths as reported earlier by Pott and McNicol for Fe^{3+} in sodalite.[41] These were assigned to transitions from the $^6A_1(^6S)$ ground state to $^4E(^4D)$ (377 nm), $^4T_2(^4D)$ (426 nm), $^4A_1,^4E(^4G)$ (450 nm), and $^4T_2(^4G)$ (517 nm) based on the assignments given by Pott and McNicol.[41] In addition to these weak bands, also an intense signal is observed at 240 nm (Figure 6c). On the basis of the data reported for Fe^{3+} in the tetrahedral site of $Y_3Al_5O_{15}$,[42] we assign this to the $O^{2-} \rightarrow Fe^{3+}$ charge transfer transition. These transitions and their related energies are further confirmed by TD-DFT calculations (Figure 6a). The CT transition overlaps significantly with the PeL excitation spectrum (Figure 6c), which means that these two compete for the excitation photons.

There may also be some Fe^{2+} present in the samples and thus we need to consider also its effects. Ravikumar et al.[43] reported that Fe^{2+} has absorption bands at 1723, 1754, 2306, and 2338 nm in sodalite. However, they gave no information about possible bands in the visible or UV ranges, i.e., such bands that would either interfere with the PeL excitation process or absorb the PeL emission. On the basis of the TD-DFT calculation of Fe^{2+} (Figure 6a) and on the Tanabe-Sugano diagram for tetrahedral Fe^{2+} (d^4 diagram, high-spin side[44]), we can assume that the NIR range absorptions are due to spin-allowed $^5E \rightarrow {}^5T_2$ transitions, whereas the transitions to higher energy states involve change in spin multiplicity and thus are generally weaker. Accordingly, Rossman and Taran[45] report no Fe^{2+} absorption bands in the visible or UV for spinel ($MgAl_2O_4$) or gehlenite ($Ca_2[Al,Fe,Mg][Si,Al]_2O_7$) either, both of which have iron substituting aluminum in a tetrahedral site. Instead, there are strong absorption bands between ca. 1850 and 2750 nm. Thus, combining the fact that Fe^{2+} is in

https://dx.doi.org/10.1021/acs.chemmater.0c02554
Chem. Mater. XXXX, XXX, XXX−XXX

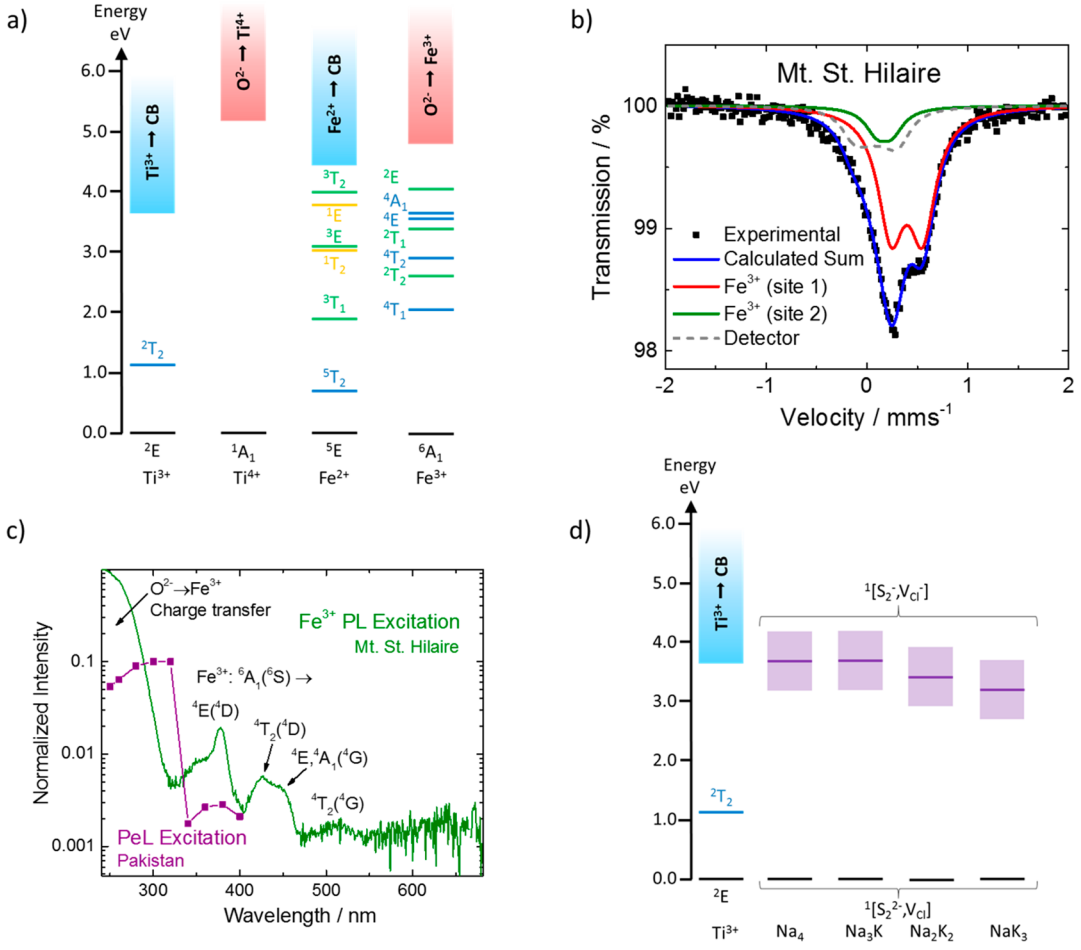

Figure 6. (a) Quantum chemically calculated energy states of Fe^{3+}, Fe^{2+}, and Ti^{3+} in the Al^{3+} site as well as Ti^{4+} in the Si^{4+} site. (b) ^{57}Fe Mössbauer spectrum of the Mt. St. Hilaire sample. (c) Photoluminescence excitation spectrum of the red Fe^{3+} band for the Mt. St. Hilaire sample (green curve) and PeL excitation spectrum of the Pakistan sample (purple curve). (d) Quantum chemically calculated energy states of Ti^{3+} (in the Al^{3+} site) as well as S_2^{2-} + V_{Cl} pair in different $Na_{4-x}K_x$ stoichiometries in hackmanite (horizontal dark purple line is the computed energy, the purple box depicts the 1 eV fwhm around the transition).

very low concentration in natural hackmanite and that possible UV−vis transitions are spin forbidden the competition of Fe^{2+} based transitions and the PeL phenomenon is expected to be rather weak. But TD-DFT calculation on Fe^{2+} reveals also the possibility of a Fe^{2+} → CB charge transfer transition partly overlapping with Ti^{3+} → CB one and thus competing with the PeL mechanism.

To get a more complete picture of the effect of the energy states of iron species, we also considered the possibility of (Fe^{3+},Ti^{3+}) and (Fe^{2+},Ti^{4+}) defects. Intervalence transitions associated with these defects are expected around 2.2−3.0 eV by DFT calculations (Figure S10), thus far from the PeL excitation wavelength. In conclusion, the main competition paths induced by iron ions for the Ti^{3+} → CB transition (responsible of the PeL) are the Fe^{2+} → CB and O^{2-} → Fe^{3+} charge transfer transitions. The possibility for Fe^{3+} to capture the trapped electron (yielding Fe^{2+}) cannot be discarded.

Interplay between Potassium and Sulfur. The quenching effect of sulfur on PeL can be explained by the fact that sulfur (i.e., the S_2^{2-} ion) is the element that absorbs radiation during the tenebrescence process. The absorption results in electron transfer from the disulfide ion to a chlorine vacancy (V_{Cl}), i.e., the creation of a color center. This color center absorbs around 550 nm (Figure 4c) causing the characteristic purple color of tenebrescent hackmanites. This tenebrescence process competes with the PeL process thus decreasing the PeL efficiency.[9] Previously, we reported, on the basis of computational data, how an increase of Na substitution by K around V_{Cl} results in a decrease of the threshold energy required for the creation of the color center.[5] Such a behavior could mean that an increased K concentration should in fact increase tenebrescence intensity (and decrease PeL). However, if we take into account the previously reported observation that the absorption connected with the creation of the color center is band-like and has a half-width of ca. 1 eV,[9] then the interplay between K and S becomes rather clear. We will explain this next.

Figure 6d shows the calculated energy states of Ti^{3+} ($Ti_{Al}^{\times}$) as well as those involved in the creation of the color center ($S_{2,Cl}'$,$V_{Cl}^{\cdot}$) when different numbers of sodium atoms have been replaced with potassium. It is clear that if there are no potassium atoms present, then there is a high overlap between the absorption band of Ti^{3+} and the band associated with the color creation. Thus, the tenebrescence process will decrease PeL efficiently and one can safely assume that the more sulfur there is the weaker will PeL be. However, when potassium is incorporated in the structure, the overlap decreases with increasing potassium concentration. Therefore, the competi-

https://dx.doi.org/10.1021/acs.chemmater.0c02554
Chem. Mater. XXXX, XXX, XXX−XXX

tion between the tenebrescence and the PeL will become weaker with increasing potassium concentration, i.e., adding enough K will cancel the deleterious effect of sulfur.

Such interplay of potassium and sulfur can also be witnessed in other natural sodalite group members. Haüyne and nosean, the sulfate end members of the group, both can exhibit S_2^- luminescence, but as far as we could check collectors' mineral databases, they show neither tenebrescence nor PeL. The missing PeL can be linked to a higher K-content[13−16] in view of the above. Regarding tenebrescence, it is not clear at present if that is due to the different anion cage structure (more sulfate, no or less Cl and also some K^+ and Ca^{2+} as cations) or the lack or difference of vacancies, possibly altering the trap system. Tugtupite, the Be-equivalent of sodalite, has a high Na/low K content and is a Cl end member, and can exhibit tenebrescence and PeL.[46,47] Lazurite, the sulfide end member of the sodalite group (of which the existence of a pure end member in nature is questioned) has no reported PeL. Tenebrescence, if present, will be concealed by the intense blue color.

CONCLUSIONS

The present work marks a new advancement in the understanding of the photonic behavior of the versatile hackmanite materials as well as the persistent luminescence phenomenon in general. During the course of the study, it became evident that the three remarkable optical properties of hackmanites—orange photoluminescence, blue persistent luminescence, and purple photochromism—are in very close correlation with each other. The delicate balance of these three phenomena is further fine-tuned either for better or for worse by the natural impurities residing in the hackmanite lattice. This explains why natural hackmanites' persistent luminescence is far weaker than that of the best synthetic ones. Nevertheless, the PeL capacity of natural hackmanites still surpasses that of many other synthetic persistent luminescence materials. Thus, the present study well illustrates the fact that even if nature does not do everything better than humans do, studying nature can offer invaluable help on how to improve the performance of synthetic materials.

ASSOCIATED CONTENT

Supporting Information

The Supporting Information is available free of charge at https://pubs.acs.org/doi/10.1021/acs.chemmater.0c02554.

Additional measurements, statistical analyses, and description of computational details (PDF)

AUTHOR INFORMATION

Corresponding Authors

Tangui Le Bahers − *Université Lyon, ENS de Lyon, CNRS, Université Lyon 1, Laboratoire de Chimie UMR, 5182 Lyon, France;* orcid.org/0000-0003-2166-081X; Email: tangui.le_bahers@ens-lyon.fr

Mika Lastusaari − *University of Turku, Department of Chemistry, FI-20014 Turku, Finland; Turku University Centre for Materials and Surfaces (MatSurf), Turku, Finland;* orcid.org/0000-0003-1872-0391; Email: miklas@utu.fi

Authors

Cecilia Agamah − *University of Turku, Department of Chemistry, FI-20014 Turku, Finland; University of Turku Graduate School (UTUGS), Doctoral Programme in Physical and Chemical Sciences, FI-20014 Turku, Finland*

Sami Vuori − *University of Turku, Department of Chemistry, FI-20014 Turku, Finland; University of Turku Graduate School (UTUGS), Doctoral Programme in Physical and Chemical Sciences, FI-20014 Turku, Finland*

Pauline Colinet − *Université Lyon, ENS de Lyon, CNRS, Université Lyon 1, Laboratoire de Chimie UMR, 5182 Lyon, France*

Isabella Norrbo − *University of Turku, Department of Chemistry, FI-20014 Turku, Finland*

José Miranda de Carvalho − *University of São Paulo, Department of Applied Physics, São Paulo, São Paulo 0508-000, Brazil;* orcid.org/0000-0002-5828-0848

Liana Key Okada Nakamura − *Colégio Nossa Senhora das Dores, São Paulo, São Paulo BR-02517-001, Brazil*

Joachim Lindblom − *Morris Lindblom & Company, FI-20200 Turku, Finland*

Ludo van Goethem − *Mineralogical Society of Antwerp, 2100 Deurne, Belgium*

Axel Emmermann − *Mineralogical Society of Antwerp, 2100 Deurne, Belgium*

Timo Saarinen − *University of Turku, Department of Geography and Geology, FI-20014 Turku, Finland*

Tero Laihinen − *University of Turku, Department of Chemistry, FI-20014 Turku, Finland*

Eero Laakkonen − *University of Turku, Department of Teacher Education, FI-20014 Turku, Finland*

Johan Lindén − *Åbo Akademi University, Faculty of Science & Engineering/Physics, FI-20500 Turku, Finland*

Jari Konu − *University of Jyväskylä, Department of Chemistry, FI-40014 Jyväskylä, Finland;* orcid.org/0000-0002-7408-8995

Henk Vrielinck − *Ghent University, Department of Solid State Sciences, Gent 9000, Belgium;* orcid.org/0000-0003-4861-9630

David Van der Heggen − *Ghent University, Department of Solid State Sciences, Gent 9000, Belgium;* orcid.org/0000-0002-6938-5573

Philippe F. Smet − *Ghent University, Department of Solid State Sciences, Gent 9000, Belgium;* orcid.org/0000-0003-4789-5799

Complete contact information is available at: https://pubs.acs.org/10.1021/acs.chemmater.0c02554

Author Contributions

▲These authors contributed equally to this work. The manuscript was written through contributions of all authors

Notes

The authors declare no competing financial interest.

ACKNOWLEDGMENTS

Mark Cole and Rob Woodside for providing Greenland and Afghan specimens. MSc Linus Silvander (Åbo Akademi University, Turku, Finland) is thanked for the SEM-EDS analyses. P.F.S. acknowledges the Special Research Fund at Ghent University (BOF-GOA Enclose project). D.V.d.H. acknowledges the UGent Special Research Fund for a doctoral scholarship (BOF16/DOC/327). J.M.C. thanks FAPESP for financial support (Project #2017/05195-5). The authors thank Jonas Joos for insightful discussions. The authors thank the SYSPROD project and AXELERA Pôle de Compétitivité for

https://dx.doi.org/10.1021/acs.chemmater.0c02554
Chem. Mater. XXXX, XXX, XXX−XXX

financial support (PSMN Data Center). The authors acknowledge the French agency ANR (TeneMod project ANR-17-CE29-0007-21) as well as Business Finland (SensoGlow project 2291/31/2017) for financial support.

REFERENCES

(1) Zahoransky, T.; Friis, H.; Marks, M. A. W. Luminescence and Tenebrescence of Natural Sodalites: A Chemical and Structural Study. *Phys. Chem. Miner.* **2016**, *43* (7), 459−480.
(2) *Handbook of Mineralogy*; Anthony, J. W., Bideaux, R. A., Bladh, K. W., Nichols, M. C., Eds.; Mineralogical Society of America: Chantilly, VA, 2001.
(3) Medved, D. B. Hackmanite and Its Tenebrescent Properties. *Am. Mineral.* **1954**, *39* (7−8), 615−629.
(4) Wight, W. The Gems of Mont Saint-Hilaire, Quebec, Canada. *J. Gemmol.* **1996**, *25* (1), 24−44.
(5) Norrbo, I.; Curutchet, A.; Kuusisto, A.; Mäkelä, J.; Laukkanen, P.; Paturi, P.; Laihinen, T.; Sinkkonen, J.; Wetterskog, E.; Mamedov, F.; Le Bahers, T.; Lastusaari, M. Solar UV Index and UV Dose Determination with Photochromic Hackmanites: From the Assessment of the Fundamental Properties to the Device. *Mater. Horiz.* **2018**, *5* (3), 569−576.
(6) International Mineralogical Association. List of Minerals. www.ima-mineralogy.org/Minlist.htm (accessed May 12, 2020).
(7) Curutchet, A.; Le Bahers, T. Modeling the Photochromism of S-Doped Sodalites Using DFT, TD-DFT, and SAC-CI Methods. *Inorg. Chem.* **2017**, *56* (1), 414−423.
(8) Armstrong, J. A.; Weller, M. T. Structural Observation of Photochromism. *Chem. Commun.* **2006**, *4* (10), 1094−1096.
(9) Norrbo, I.; Gluchowski, P.; Hyppänen, I.; Laihinen, T.; Laukkanen, P.; Mäkelä, J.; Mamedov, F.; Santos, H. S.; Sinkkonen, J.; Tuomisto, M.; Viinikanoja, A.; Lastusaari, M. Mechanisms of Tenebrescence and Persistent Luminescence in Synthetic Hackmanite $Na_8Al_6Si_6O_{24}(Cl, S)_2$. *ACS Appl. Mater. Interfaces* **2016**, *8* (18), 11592−11602.
(10) Gaft, M.; Panczer, G.; Nagli, L.; Yeates, H. Laser-Induced Time-Resolved Luminescence of Tugtupite, Sodalite and Hackmanite. *Phys. Chem. Miner.* **2009**, *36* (3), 127−141.
(11) Aierken, S.; Kusachi, I.; Kobayashi, S.; Atobe, K.; Yamashita, N. Photoluminescence Spectra of S_2^- Center in Natural and Heat-Treated Scapolites. *Phys. Chem. Miner.* **2008**, *35* (3), 137−145.
(12) Colinet, P.; Gheeraert, A.; Curutchet, A.; Le Bahers, T. On the Spectroscopic Modeling of Localized Defects in Sodalites by TD-DFT. *J. Phys. Chem. C* **2020**, *124* (16), 8949−8957.
(13) Lessing, P.; MacDonald Grout, C. Haünite from Edwards, New York. *Am. Mineral.* **1971**, *56*, 1096−1100.
(14) Wulff-Pedersen, E.; Neumann, E.-R.; Burke, E. A. J.; Vannucci, R.; Bottazzi, P.; Ottolini, L.; Gjønnes, J.; Hansen, V. Origin and Structural Character of Haüyness in Spinel Dunite Xenoliths from La Palma, Canary Islands. *Am. Mineral.* **2000**, *85*, 1397−1405.
(15) Balassone, G.; Bellatreccia, F.; Ottolini, L.; Mormone, A.; Petti, C.; Ghiara, M. R.; Altomare, A.; Saviano, M.; Rizzi, R.; D'Orazio, L. Sodalite-Group Minerals from the Somma-Vesuvius Volcano (Naples, Italy): A Combined EPMA, SIMS, and FTIR Crystal-Chemical Study. *Can. Mineral.* **2016**, *54* (3), 583−604.
(16) Di Muro, A.; Bonaccorsi, E.; Principe, C. Complex Colour and Chemical Zoning of Sodalite-Group Phases in a Haüynophyre Lava from Mt. Vulture, Italy. *Mineral. Mag.* **2004**, *68* (4), 591−614.
(17) Burgner, R. P.; Scheetz, B. E.; White, W. B. Vibrational Structure of the S_2^- Luminescence in Scapolite. *Phys. Chem. Miner.* **1978**, *2*, 317−324.
(18) Blumentritt, F.; Latouche, C.; Morizet, Y.; Caldes, M.-T.; Jobic, S.; Fritsch, E. Unravelling the Origin of the Yellow-Orange Luminescence in Natural and Synthetic Scapolites. *J. Phys. Chem. Lett.* **2020**, *11* (12), 4591−4596.
(19) Warner, T. E. *Synthesis, Properties and Mineralogy of Important Inorganic Materials*; Wiley: Somerset, 2016.
(20) Marfunin, A. S. *Spectroscopy, Luminescence and Radiation Centers in Minerals*; Springer: Berlin, 1979.
(21) Wu, S.; Pan, Z.; Chen, R.; Liu, X. *Long Afterglow Phosphorescent Materials*; Springer: Cham, 2017.
(22) Norrbo, I.; Carvalho, J. M.; Laukkanen, P.; Mäkelä, J.; Mamedov, F.; Peurla, M.; Helminen, H.; Pihlasalo, S.; Härmä, H.; Sinkkonen, J.; Lastusaari, M. Lanthanide and Heavy Metal Free Long White Persistent Luminescence from Ti Doped Li−Hackmanite: A Versatile, Low-Cost Material. *Adv. Funct. Mater.* **2017**, *27* (17), 1606547.
(23) Deutsche Norm. Phosphorescent Pigments and Products—Part 1: Measurement and Marking at the Producer. **2009**; p DIN 67510-1:2009-11.
(24) Norrbo, I.; Gluchowski, P.; Paturi, P.; Sinkkonen, J.; Lastusaari, M. Persistent Luminescence of Tenebrescent $Na_8Al_6Si_6O_{24}(Cl, S)_2$: Multifunctional Optical Markers. *Inorg. Chem.* **2015**, *54* (16), 7717−7724.
(25) Chen, R.; Pagonis, V. *Thermally and Optically Stimulated Luminescence: A Simulation Approach*; Wiley: Sussex, 2011.
(26) Van der Heggen, D.; Joos, J. J.; Rodriguez Burbano, D. C.; Capobianco, J. A.; Smet, P. F. Counting the Photons: Determining the Absolute Storage Capacity of Persistent Phosphors. *Materials* **2017**, *10* (8), 867.
(27) Dovesi, R.; Erba, A.; Orlando, R.; Zicovich-Wilson, C. M.; Civalleri, B.; Maschio, L.; Rerat, M.; Casassa, S.; Baima, J.; Salustro, S.; et al. Quantum-Mechanical Condensed Matter Simulations with CRYSTAL. *WIREs Comput. Mol. Sci.* **2018**, *8*, No. e1360.
(28) Adamo, C.; Barone, V. Toward Reliable Density Functional Methods without Adjustable Parameters: The PBE0Model. *J. Chem. Phys.* **1999**, *110* (13), 6158−6170.
(29) Frisch, M. J.; Trucks, G. W.; Schlegel, H. B.; Scuseria, G. E.; Robb, M. A.; Cheeseman, J. R.; Scalmani, G.; Barone, V.; Petersson, G. A.; Nakatsuji, H.; Li, X.; Caricato, M.; Marenich, A. V.; Bloino, J.; Janesko, B. G.; Gomperts, R.; Mennucci, B.; Hratchian, H. P.; Ortiz, J. V.; Izmaylov, A. F.; Sonnenberg, J. L.; Williams-Young, D.; Ding, F.; Lipparini, F.; Egidi, F.; Goings, J.; Peng, B.; Petrone, A.; Henderson, T.; Ranasinghe, D.; Zakrzewski, V. G.; Gao, J.; Rega, N.; Zheng, G.; Liang, W.; Hada, M.; Ehara, M.; Toyota, K.; Fukuda, R.; Hasegawa, J.; Ishida, M.; Nakajima, T.; Honda, Y.; Kitao, O.; Nakai, H.; Vreven, T.; Throssell, K.; Montgomery, J. A. J.; Peralta, J. E.; Ogliaro, F.; Bearpark, M. J.; Heyd, J. J.; Brothers, E. N.; Kudin, K. N.; Staroverov, V. N.; Keith, T. A.; Kobayashi, R.; Normand, J.; Raghavachari, K.; Rendell, A. P.; Burant, J. C.; Iyengar, S. S.; Tomasi, J.; Cossi, M.; Millam, J. M.; Klene, M.; Adamo, C.; Cammi, R.; Ochterski, J. W.; Martin, R. L.; Morokuma, K.; Farkas, O.; Foresman, J. B.; Fox, D. J. *Gaussian 16*; Gaussian, Inc.: Wallingford CT, 2016.
(30) Yanai, T.; Tew, D. P.; Handy, N. C. A New Hybrid Exchange-Correlation Functional Using the Coulomb-Attenuating Method (CAM-B3LYP). *Chem. Phys. Lett.* **2004**, *393* (1−3), 51−57.
(31) Serway, R. A.; Marshall, S. A. Electron Spin Resonance Absorption Spectra of CO_3^- and CO_3^{3-} Molecule—Ions in Irradiated Single-Crystal Calcite. *J. Chem. Phys.* **1967**, *46*, 1949−1952.
(32) Evans, B. D.; Pogatshnik, G. J.; Chen, Y. Optical Properties of Lattice Defects in (-Al_2O_3. *Nucl. Instrum. Methods Phys. Res., Sect. B* **1994**, *91* (1994), 258−262.
(33) Zorenko, Y.; Zorenko, T.; Voznyak, T.; Mandowski, A.; Xia, Q.; Batentschuk, M.; Friedrich, J. Luminescence of F + and F Centers in Al_2O_3-Y_2O_3 Oxide Compounds. *IOP Conf. Ser.: Mater. Sci. Eng.* **2010**, *15*, 012060.
(34) Kristianpoller, N.; Rehavy, A. Luminescence Centers in Al_2O_3. *J. Lumin.* **1979**, *19*, 239−243.
(35) Wagatsuma, K.; Hirokawa, K. Characterization of Atomic Emission Lines from Argon, Neon, and Nitrogen Glow Discharge Plasmas. *Anal. Chem.* **1985**, *57* (14), 2901−2907.
(36) Ghamnia, M.; Jardin, C.; Bouslama, M. Luminescent Centres F and F+ in α-Alumina Detected by Cathodoluminescence Technique. *J. Electron Spectrosc. Relat. Phenom.* **2003**, *133* (1−3), 55−63.
(37) International Centre for Diffraction Data. Sodalite $Na_8(Al_6Si_6O_{24})Cl_2$. *Powder Diffr. File* **2018**, Entry No. 01-086-1844.

https://dx.doi.org/10.1021/acs.chemmater.0c02554
Chem. Mater. XXXX, XXX, XXX−XXX

(38) van den Brom, W. E.; Kerssen, J.; Volger, J. Electric Dipole Centres and Colour Centres in Natural Sodalite. *Physica* **1974**, *77*, 1−26.
(39) Gaft, M.; Reisfeld, R.; Panczer, G. *Luminescence Spectroscopy of Minerals and Materials*; Springer: Berlin, 2005.
(40) Goldfarb, D.; Bernardo, M.; Strohmaier, K. G.; Vaughan, D. E. W.; Thomann, H. Characterization of Iron in Zeolites by X-Band and Q-Band ESR, Pulsed ESR, and UV-Visible Spectroscopies. *J. Am. Chem. Soc.* **1994**, *116* (14), 6344−6353.
(41) Pott, G. T.; McNicol, B. D. Phosphorescence of Fe^{3+} Ions in Oxide Host Lattices. Zero-Phonon Transitions in $Fe^{3+}/LiAl_5O_8$. *Chem. Phys. Lett.* **1971**, *12* (1), 62−64.
(42) Chen, C. Y.; Pogatshnik, G. J.; Chen, Y.; Kokta, M. R. Optical and Electron Paramagnetic Resonance Studies of Fe Impurities in Yttrium Aluminum Garnet Crystals. *Phys. Rev. B: Condens. Matter Mater. Phys.* **1988**, *38* (13), 8555−8561.
(43) Ravikumar, R. V. S. S. N.; Chandrasekhar, a. V.; Yamauchi, J.; Reddy, Y. P.; Rao, P. S. Tetrahedral Site of Iron in Natural Mineral Sodalite. *Radiat. Eff. Defects Solids* **2005**, *160* (3−4), 109−115.
(44) Atkins, P.; Overton, T.; Rourke, J.; Weller, M.; Armstrong, F.; Hagerman, M. *Shriver & Atkins Inorganic Chemistry*, 5th ed.; W.H. Freeman and Company: New York NY, 2010.
(45) Rossman, G. R.; Taran, M. N. Spectroscopic Standards for Four- and Fivefold-Coordinated Fe^{2+} in Oxygen-Based Minerals. *Am. Mineral.* **2001**, *86* (7−8), 896−903.
(46) Warner, T. E.; Andersen, J. H. The Effects of Sulfur Intercalation on the Optical Properties of Artificial 'Hackmanite', $Na_8[Al_6Si_6O_{24}]Cl_{1.8}S_{0.1}$; 'Sulfosodalite', $Na_8[Al_6Si_6O_{24}]S$; and Natural Tugtupite, $Na_8[Be_2Al_2Si_8O_{24}](Cl, S)_{2-\delta}$. *Phys. Chem. Miner.* **2012**, *39* (2), 163−168.
(47) Antao, S. M.; Hassan, I. Thermal Analyses of Sodalite, Tugtupite, Danalite and Helvite. *Can. Mineral.* **2002**, *40* (1), 163−172.

https://dx.doi.org/10.1021/acs.chemmater.0c02554
Chem. Mater. XXXX, XXX, XXX−XXX